

Experimental study of quasiperiodicity in a hydrodynamical system

Joel Stavans*

The James Franck Institute, The University of Chicago, 5640 Ellis Avenue, Chicago, Illinois 60637

(Received 26 September 1986)

In this paper we present an experimental study of quasiperiodicity in a hydrodynamical system. Partial results have already been reported. We present them now in more detail as well as the experiment itself. The system studied is Rayleigh-Bénard convection in mercury in a time-dependent state with one limit cycle. An external oscillation is coupled to this limit cycle by passing an ac electrical current through the mercury and embedding the system in a horizontal magnetic field. We have measured the fractal dimension of the complement of all locked states on the critical line. Local properties of this line, such as scaling indices, were also measured for two different irrational routes followed. The results are in good agreement with quantitative predictions of the circle map.

I. INTRODUCTION

In this paper we present an experimental study of quasiperiodicity in Rayleigh-Bénard convection. In quasiperiodicity one studies the behavior of a set of nonlinearly coupled oscillators. The simplest case, two oscillators, is the one we will report here.

When the amplitude of the nonlinear interaction coupling the oscillators is small, the system can be in one of two possible states. The oscillators are in a quasiperiodic state if the ratio of their frequencies or winding number is an irrational number. Otherwise, the oscillators are said to be locked and the winding number is rational. Locked states have the following property: if one changes the frequency or the amplitude of one oscillator within a given range of variation, the second oscillator readjusts its respective parameters so that the winding number does not change. This range of variation increases with the amplitude of the nonlinear coupling.

The possible states of the system can be conveniently parametrized in the amplitude-versus-frequency plane of one of the oscillators. In this plane, the locked states appear as regions called "Arnol'd tongues." There is a tongue for every rational number. The width of each tongue at fixed amplitude is a rapidly decreasing function of the denominator of the particular rational number. The tongues that appear in this plane are ordered through the Farey scheme, which will be explained in detail in later sections.

Because the frequency width of the Arnol'd tongues increases with the amplitude, eventually the tongues overlap. In the region where the tongues overlap, the state of the system is not uniquely defined by the amplitude and frequency values but also by its past history. Hysteretic effects appear. Moreover, the system can exhibit chaotic behavior both inside and outside tongues.

In this paper we have focused our attention on the region in the amplitude-versus-frequency plane below and at the critical line where the tongues start to overlap. We have mapped out a number of Arnol'd tongues and measured global and local properties of the overlap line. We have also studied the transition to chaotic behavior when

the winding number is fixed to an irrational value and the amplitude of one oscillator is increased towards the overlap line. Of course, an irrational frequency ratio cannot be achieved experimentally, but given our resolution and stability, we have been able to approximate it within 10^{-4} .

In order to fulfill this program and explore the amplitude-frequency plane, one must be able to have under one's control the amplitude and frequency of one of the oscillators. Usually, the amplitude and frequency are not independent. A change in the amplitude of one oscillator will then induce changes in the frequencies of both oscillators. Since keeping the winding number constant is essential for comparing our results to existing models for the quasiperiodic transition to chaos, this control is also necessary from the experimental point of view. This stands in contrast to experimental observations of period doubling and intermittency, where only the change in one parameter suffices to observe the whole scenario.

To achieve this, we have devised a forced convection experiment in liquid mercury in a cell of small aspect ratio. In this way, most spatial modes are frozen and the time domain is singled out. One of the oscillators is the local oscillation of the fluid for high enough Rayleigh number, while the second is imposed from the outside by embedding the system in a uniform magnetic field and passing an ac electrical current sheet through the fluid. The induced Lorentz force acts directly upon the fluid's velocity field. Since the current is imposed from the outside, its frequency and amplitude are at our disposal.

One can then study the response of the fluid as a function of these two parameters. A signal is obtained from the experiment by means of a local thermal probe. The analysis of the experimental data is carried out by performing Fourier spectra of the signal and by studying the Poincaré cross sections of the dynamical trajectories.

As usual in these types of problems it is impossible to develop a theoretical model starting with the Navier-Stokes and Fourier heat equations. The theoretical analysis consists of comparing the experimental results with those obtained from a simple dynamical system. The model dynamical system is a one-dimensional map of the circle onto itself. The relevance of such a map to our ex-

periment can be seen from the following facts. A system of two oscillators describes in phase space a trajectory on a torus. When the torus is cut by a Poincaré plane, the trajectory cuts the plane in points lying on a curve topologically equivalent to a circle.

Although results from these circle maps were known to mathematicians through the works of Arnol'd, Herman, Denjoy, and others,¹⁻³ it was not possible to make quantitative comparisons with experiment until the development of renormalization-group techniques applied to dynamical systems.⁴ In the case of the circle map, these techniques were applied⁵⁻⁷ while a considerable amount of knowledge was being amassed from important numerical studies.^{8,9}

The justification for our procedure of analysis is the assumption of the universality of the results in the same spirit as for critical phenomena.

The first attempt to observe experimentally the transition to chaos via quasiperiodicity was done by Fein, Heutmaker, and Gollub,¹⁰ who obtained evidence of the scaling properties of the spectrum. Their system, however, did not allow them to obtain quantitative properties such as critical indices or global properties of the amplitude-frequency plane.

Recently, we reported an experimental observation of the transition to chaos via quasiperiodicity and fixed winding number.¹¹ It is the purpose of this paper to give a more detailed account of both the results and the experiment. The layout of the paper is the following. In Sec. II we review the salient features of Rayleigh-Bénard convection relevant to our experiment and describe briefly the circle map. In Sec. III we describe the experimental setup and the motivations which led to its particular design. In Sec. IV we present our results and compare them with the predictions of the circle map. Finally, in Sec. V we present our conclusions and future perspectives.

II. THEORY

A. Rayleigh-Bénard convection

Our experiment was performed with mercury as the convecting fluid. One important property of mercury is its low Prandtl number P defined as the ratio between the kinematic viscosity and the heat diffusivity. In the case of mercury $P=0.025$. Among the properties of fluids of low Prandtl number is the appearance of a temporal oscillatory mode when the fluid is heated above the convection onset.¹² This mode is an instability of the convection pattern rather than a detachment of boundary layers, which occurs in large-Prandtl-number fluids. Since this mode is one of the two oscillators in the experiment, we give now a brief description of it. We also explain why the experiment was performed in a small aspect ratio.

In a Rayleigh-Bénard experiment one has a layer of fluid bounded on top and bottom by two horizontal plates. The temperature of the bottom plate is higher than that of the top plate. If the temperature gradient across the layer is small, the heat is transported by diffusion. If on the other hand the gradient is sufficiently large, convection sets in. This situation is described by two equations: the

Navier-Stokes momentum equation and the Fourier heat equation. Assuming incompressibility and a set of fluid characteristics which is commonly encountered, a considerable simplification of these equations (the Boussinesq approximation) is possible. Upon recasting the simplified equations nondimensionally, one arrives at a description of thermal convection by means of two independent nondimensional parameters: the Rayleigh number R and the Prandtl number P . R includes geometrical factors of the system and is proportional to the temperature gradient across the layer. P is an intrinsic property of the fluid and is independent of the setup.

When convection sets in at $R=R_c$, the only stable cellular pattern consists of horizontal parallel rolls with adjacent rolls rotating in opposite directions. The width of each roll is of order d , the separation between the top and bottom plates. The cross section of a convective roll is then approximately square.

As R is increased above R_c , the convection pattern goes through a series of instabilities reaching eventually chaotic temporal behavior. The nature of these instabilities is different for different fluids and what essentially determines which instabilities the system will go through is the Prandtl number P .¹²

A linear-stability analysis of the equations of motion shows that above R_c a continuous band of modes is accessible to the system. A nonlinear analysis shrinks this band but does not select a particular mode of the system.

It is at this point that we have to distinguish between two possible physical situations: one in which the horizontal dimensions of the system are much larger than d (large aspect ratio), and one in which the horizontal extent is comparable to d (small aspect ratio).

For large aspect ratio, the modal interaction manifests itself in the presence of defects and wavelength variations in the convective pattern. Moreover, such convective patterns are not stationary and evolve aperiodically over very long time scales.¹³⁻¹⁵ This broadens the spectral features and increases the noise level, particularly at small frequencies, rendering the system unusable for our purposes.

In the case of small aspect ratio, the influence of the walls is strongly felt throughout the bulk. The walls effectively damp out most degrees of freedom, and the convection pattern is that of a small number of straight rolls without defects.

For small-Prandtl-number fluid, the first instability after convection is a time-dependent mode called the oscillatory instability. In this mode the rolls bend transversally to the direction of their axes with a well-defined temporal ratio. The characteristic time scale for this period is given by $\tau \sim d^2/\kappa$, where κ is the heat diffusivity of the fluid. A very important feature of the oscillatory instability is that after it sets in, the fluid flow is three dimensional. Below threshold, the rolls are straight and the flow is essentially two dimensional. Thus the vorticity of the flow which is parallel to the rolls below the instability acquires an ac vertical component above the instability threshold. Thus, the instability and vertical vorticity are intimately related. This was pointed out first by Busse.¹⁶ For infinite layers Busse showed that this instability is caused by the nonlinear term in the Navier-Stokes equa-

tion; this term, which is the dominant nonlinearity in the limit of small Prandtl numbers, is the only one capable of inducing vertical vorticity in the flow. Moreover, Busse showed that the instability appears after the amplitude of the convection exceeds some critical value.

Comparing the advection and diffusion terms in the Navier-Stokes equation, one can define a Reynolds number for the flow

$$\mathcal{R} = \frac{uL}{\nu},$$

where u and L are typical velocity and length scales. ν is the kinematic viscosity. Busse's conclusion about the finite-amplitude onset is then equivalent to the existence of a critical Reynolds number above which the instability sets in. Therefore, while the onset of convection is associated with a critical Rayleigh number, the onset of the oscillatory instability is associated with a critical value of the Reynolds number.

Siggia and Zippelius¹⁷ have studied the stability of rolls within the framework of amplitude equations.^{18,19} They showed that the Newell-Whitehead-Segel equation is insufficient to determine correctly the instabilities and must be supplemented with an extra coupled equation that describes the evolution of a large-scale flow. By large scale, we mean a scale larger than the roll wavelength. This flow is the one which possesses vertical vorticity. The interaction between the small-scale cellular pattern and the large-scale flow induces the instability.

Using these ideas, one easily obtains for the instability onset

$$\sqrt{R - R_c} \sim aP,$$

where a is the wave vector of the convective structure. This brings out the importance of P in determining the onset of the instability. In addition, one can also make a prediction about the frequency of the oscillatory instability,

$$\omega \sim \frac{\kappa}{d^2} \sqrt{R - R_c}.$$

If R is increased further, eventually a second frequency appears and the two internal oscillators interact nonlinearly. The nature of this second oscillatory mode is still not understood. It might be associated with a dephasing of the rolls' motion.

Two cases are then possible: either the frequency ratio of the two oscillators is an irrational number or a rational one. We refer to the frequency ratio as the winding number. In the former case, or quasiperiodic state, the experimental signal shows a beating pattern between the two frequencies. Moreover, as R is changed, both frequencies change independently so that their ratio changes as well. When the winding number is rational we say that the system is in a locked state, and one observes a periodic signal from the experiment. A locked state exists for a finite range of R ; as R is changed within this range, both oscillators change their frequencies keeping the winding number fixed.

What is typically observed in an experiment is that as R is increased, the two oscillators lock and unlock succes-

sively until they fall in a locked state in which a period-doubling cascade occurs.²⁰ This cascade leads to chaotic behavior. At other times, the system becomes chaotic through the appearance of a third frequency.

It is then natural to ask how quasiperiodic states become chaotic. To answer this, one has to be able to control at least one of the frequencies in the problem, so that the frequency ratio is an irrational number and therefore locked states can be avoided. In analogy to the locked states, one would like to keep the frequency ratio constant. We accomplished this by fixing R so that only one oscillator is present in the fluid. We then imposed a second, external oscillation, whose amplitude and frequency were at our disposal. Our first attempts at imposing an external oscillator did not lead to interesting results because the external oscillator did not couple dynamically with the oscillatory instability, a task which turned out to be nontrivial. As we will see, the excitation itself has to induce vertical vorticity in the flow.

There is an essential difference between our experiment and one in which the two oscillators are a result of flow instabilities: when both oscillators are flow generated, there is feedback between the two. In our case the interaction is one sided: the external oscillator acts on the internal one but not *vice versa*. The amplitude and frequency of the external oscillator are imposed.

The three main conclusions from this section, which were taken into account in our experimental design, are the following. First, a small-aspect-ratio cell freezes out complicated spatial modes and isolates the temporal dynamics. Second, a low-Prandtl-number fluid generates an oscillatory mode intrinsic to the convection pattern. In our case, we used mercury, taking advantage of its electrical conductivity to introduce our excitation. The advantages of using electromagnetic methods as opposed to thermal ones will become clear in the sequel. Last but not least, in order to study the quasiperiodic transition to chaos, one of the two oscillators in the experiment must be an external one. In this way, one can keep the winding number constant when changing the nonlinearities in the system.

B. The circle map

Theoretical studies of the transition to chaos via quasiperiodicity with fixed winding number have focused on maps of the circle onto itself. In this section we motivate the relevance of these maps to our experiment and how they arise phenomenologically. We then survey circle-map studies and their theoretical predictions following closely the paper by Jensen, Bak, and Bohr.²¹

We consider a dissipative nonlinear oscillator that is forced by a periodic external excitation. We can think of this system as one of two oscillators interacting nonlinearly via a one-directional interaction. The meaning of this is that a dynamical parameter (i.e., amplitude) of the first oscillator enters the equation of motion of the second while the first oscillator is unaffected by the second.

With this picture in mind, it is easy to see that the system moves in phase space on a two-torus which is the product of phase spaces (circles) of each of the two oscil-

lators. Unlike the analogous Kol'mogorov-Arnol'd-Moser (KAM) tori of nonlinear conservative systems, the torus under consideration is an attractor of the motion in the sense that nearby phase-space orbits converge to it.

Thus one studies the dynamical behavior of the physical system by considering the different types of orbits on the torus. These can be grouped in two classes. If the frequency ratio of both oscillators is a rational number, then the orbit on the torus is a closed curve. If on the other hand the ratio is an irrational number, the orbit does not close and fills the surface of the torus densely.

It turns out that one can simplify the problem considerably and still retain the essential dynamical information if one makes use of a construction due to Poincaré, which effectively reduces the dimension of the problem by one.²² The idea is to look at a cross section (Poincaré cross section) of the torus, obtained by cutting it with a surface. This surface need not necessarily be a plane but the orbits should cross it transversally. The meaning of transversality here is that no orbit intersecting the surface is tangent to it.

The intersection of the orbits and the surface is a curve which is topologically equivalent to a circle. If the orbit on the torus corresponds to a rational number p/q , the Poincaré cross section will consist of a discrete set of q points. If the orbit is quasiperiodic, i.e., the winding number is irrational, the circle will be densely filled.

The dynamics of the physical system is then reduced to the study of the Poincaré cross section. One does this by building a return map of the circle onto itself, i.e., a functional relationship between the angular coordinate parametrizing the circle at the n th crossing θ_n , and the one at the $(n+1)$ th crossing θ_{n+1} . Mathematically, the procedure outlined above takes the following form. One starts from an equation describing a periodically excited nonlinear dissipative oscillator in the variable θ . Being of second order, one recasts it as a system of two first-order differential equations in the variables $\theta, \dot{\theta}$. One then constructs a return map M between the values of $\theta, \dot{\theta}$ at the beginning of the n th period of the excitation, and their values at the end of the period. Denoting by $\theta_n, \dot{\theta}_n$ the values of $\theta, \dot{\theta}$ at the time nT we have

$$\begin{pmatrix} \theta_{n+1} \\ \dot{\theta}_{n+1} \end{pmatrix} = M \begin{pmatrix} \theta_n \\ \dot{\theta}_n \end{pmatrix} = \begin{pmatrix} f_1(\theta_n, \dot{\theta}_n) \\ f_2(\theta_n, \dot{\theta}_n) \end{pmatrix},$$

where the f_i are periodic in θ_n . Since the original equation includes a dissipative term, the Jacobian of the transformation is smaller than one, i.e., the map is area contracting. The information on the initial conditions is lost asymptotically. In other words, the motion on the torus is asymptotically an invariant curve which depends only on the time $\theta(t)$. In particular, θ will be a function of θ ,

$$\dot{\theta}_n = g(\theta_n).$$

Substituting this relation in the above equation yields:

$$\theta_{n+1} = F(\theta_n) = f_1(\theta_n, g(\theta_n)),$$

which is a one-dimensional map of a circle onto itself.

The map which is most often considered because of its simplicity is the sine circle map,

$$\theta_{n+1} = f(\theta_n) = \theta_n + \Omega - (K/2\pi) \sin(2\pi\theta_n).$$

For $0 \leq K < 1$, f is a diffeomorphism (differentiable map with differentiable inverse) whereas for $K \geq 1$, f^{-1} does not exist. At $K=1$ the inverse exists but is not differentiable at $\theta=0$.

The rotation or winding number is mathematically defined by

$$\sigma = \lim_{n \rightarrow \infty} \left[\frac{f^{(n)}(\theta)}{n} \right].$$

For $K=0$, $\sigma = \Omega$ while for $K \neq 0$, Ω has to be adjusted to achieve a particular value of σ .

As we shall later see, the qualitative features of the transition to chaos with σ having an irrational value are the same for all irrationals. Quantitatively this is not true and in particular, the critical indices associated with the transition are different for different irrational values of σ . Before discussing the transition itself, we will first examine the global properties of the map on the (Ω, K) parameter space.

For $0 \leq K < 1$ it has been shown that for every rational p/q where p, q are mutually prime there exists a finite interval of Ω values for which $\sigma = p/q$. When this happens, the sequence $\{\theta_n\}$ is periodic $\theta_{n+q} = \theta_n + p$, and corresponds to a closed curve on the torus. One then has a locked state. For σ irrational, the corresponding value of Ω is unique. For small K , the intervals of Ω corresponding to rational winding numbers are very small. So if a random value of Ω is chosen, σ will most likely be an irrational. When K is increased, the width of every Ω interval where a locked mode occurs increases, and the probability of getting an irrational value of σ decreases. Eventually these intervals overlap when K is further increased, the overlapping starting at $K=1$.

The regions in parameter space (Ω, K) where σ is rational are called Arnol'd tongues. They are shown in Fig. 1, which is adapted from Ref. 17. Each tongue is characterized by a rational number p/q with p, q mutually prime. The tongues are ordered through the Farey scheme for rational numbers: given two rational numbers (parents) $p/q < p'/q'$, one defines their Farey composition (daughter) as

$$\frac{p}{q} \oplus \frac{p'}{q'} = \frac{p+p'}{q+q'}.$$

The daughter has two important properties. First, it obeys

$$\frac{p}{q} < \frac{p+p'}{q+q'} < \frac{p'}{q'}.$$

Second, the daughter has the smallest denominator among all the rationals between both parents. In order for all tongues to fit within the unit interval, the tongue widths have to decrease sufficiently fast for a given value of K . Jensen, Bak, and Bohr²¹ have obtained by numerical means a scaling law for the tongue widths at $K=1$. For a given value of the denominator q , they averaged the

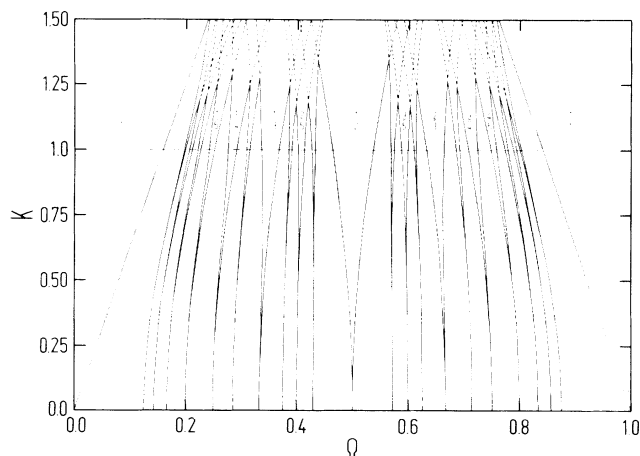


FIG. 1. Parameter space K, Ω for the one-dimensional circle map. K is the strength of the nonlinearity while Ω is the winding number. The horn regions are called Arnol'd tongues and each one is uniquely characterized by a rotational number p/q where p and q are mutually prime integers. Within a tongue, successive iterations of the map yield a periodic limit cycle the length of which is given by the denominator q . Outside tongues the signal is quasiperiodic. The line at which the tongues just intersect is called the critical line and is given by $K = 1$.

widths of all tongues with numerators $p = 1, 2, \dots, q - 1$. By repeating this procedure for different values of q they obtained that the tongue widths scale on the average as $q^{-2.29}$.

At $K = 1$, the complement of the set of Ω intervals corresponding to locked modes forms a Cantor-like set whose dimension D has been calculated numerically.⁸ Convincing evidence for the globality of this dimension on all the $K = 1$ line has been obtained by means of renormalization-group methods.²³ Both the global nature of D and D itself are universal, i.e., independent of the map f as long as it has a cubic inflection point. This is very important experimentally since the precise map corresponding to the experiment is not known.

The previous discussion summarizes the global properties of the map for $K < 1$. We now discuss the way in which the transition takes place when σ is a fixed irrational number and K approaches one. In doing so, we follow Shenker's paper.⁹

Because of the infinite limit in the definition of σ , it is impossible to determine the value of Ω which produces a particular irrational value of σ . On the other hand, when σ is a rational, there is a finite interval of values of Ω that produces the same value of σ . This suggests that to study an irrational winding number one should use a sequence of rational numbers that converge to it. It turns out that the best way of doing this is by truncating the irrational's continued-fraction representation. If ρ is an irrational number, its (unique) continued-fraction representation is

$$\rho = \frac{1}{n_1 + \frac{1}{n_2 + \frac{1}{n_3 + \dots}}}$$

and we denote it by $\rho = \langle n_1, n_2, n_3, \dots \rangle$. For reasons that will become clearer later, we limit ourselves to irrational numbers with periodic continued-fraction representations, i.e., those for which there is an integer m such that $n_i = n_{i+m}$ for all i . Theoretical studies have focused on the "golden mean"

$$\rho = \sigma_G = \langle 1, 1, 1, 1, \dots \rangle = (\sqrt{5} - 1)/2.$$

Since only ones appear in the representation of σ_G , the rational truncations of this irrational number have the slowest possible convergence. For $\rho = \sigma_G$, the rational approximants ρ_i are ratios of Fibonacci numbers,

$$\rho_i = \frac{F_i}{F_{i+1}} = \langle 1, 1, 1, 1, 1 \rangle,$$

where there are i ones in the brackets. The Fibonacci numbers F_i are defined recursively by $F_{i+2} = F_i + F_{i+1}$ for $i \geq 2$ with $F_0 = 0$ and $F_1 = 1$. Another irrational number frequently used is the "silver mean"

$$\sigma_S = \langle 2, 2, 2, 2, \dots \rangle = \sqrt{2} - 1.$$

Two mathematical results are of importance in the analysis of the map f . The first, due to Denjoy,³ states that if f is a diffeomorphism and ρ an irrational number, then f is equivalent to a uniform rotation by ρ . In mathematical terms, there exists a function $h(t)$, the "conjugation" function such that

$$h^{-1} \circ f \circ h = t + \rho,$$

where the \circ binary operation denotes functional composition. h also obeys the conditions $h(t+1) = h(t) + 1$ and $h(0) = 0$. The second result due to Herman² asserts that for almost all irrationals, h is an analytic function.

In our case, f is a diffeomorphism for $K < 1$ and the function loses its invertibility at $K = 1$. The breakdown of these results when K approaches 1 must be reflected in the behavior of $h(t)$. Thus one can study h instead of f in this limit. To do this, it is convenient to study the periodic function

$$u(t) = h(t) - t$$

and its Fourier transform $A(\omega)$.

The strategy adopted by Shenker to study numerically the function $u(t)$ and its spectrum relies heavily on the fact that one has at one's disposal a well-defined algorithm to approximate an irrational number ρ by a sequence of rationals ρ_i . For our problem, the ρ_i are the successive truncations of the continued fraction representation of ρ .

In the same spirit as one approximates ρ by ρ_i , one defines for the corresponding i th locked states a discrete set of times $\{t_j\}$ and functions $u_i(t_j)$, $A_i(\omega)$ hoping that the behavior of these reflects that of $u(t)$ and $A(\omega)$ for large i .

Shenker studied the functions $u_i(t)$ and $A_i(\omega)$ for $i = 17$. For $K < 1$, he found a very smooth curve for u_i . As K approaches one, u_i acquires an increasingly fine scale which strongly suggests self-similarity.

The behavior of the spectrum is more instructive. For $K = 0.5$ the spectrum shows peaks at values of ω corre-

sponding to small Fibonacci numbers and their amplitudes decay exponentially with ω . As K increases, new peaks appear at higher Fibonacci numbers as well as at combinations of the form $mF_i + nF_j$ with integers m, n . The number of possible combinations increases with K as well. Finally, at $K = 1$, one observes peaks at all Fibonacci numbers and all their integer combinations. Moreover the amplitude decay is proportional to $1/\omega$ instead of exponential.

Using this fact, one can rescale the spectrum at $K = 1$ to show a very appealing structure. Plotting $|\omega A(\omega)|$ versus $\ln(\omega)$, one observes the spectrum to be divided into almost identical bands flanked by strong peaks corresponding to adjacent Fibonacci frequencies. As one looks at higher ω , the bands resemble more one another in their structure and their width tends to a constant. This is just an expression of the fact that ratios of adjacent Fibonacci numbers tend to the golden mean. It is in this way that the self-similarity of $u(t)$ manifests itself in its spectrum $A(\omega)$. However, we will not discuss Shenker's version of the rescaled spectrum further since it cannot be compared with experimental spectra in a straightforward way. His frequency ω is not really a physical frequency. The reason for this is his particular definition of the Fourier transform. An alternative definition of the spectrum has been used by Rand *et al.*⁵ They also discuss the relation between both definitions and the advantages of their formulation. Since the spectrum as defined by these authors can be readily compared with our experimental results, we discuss the rescaled version in their formulation. In the sequel we denote again by A their spectrum and by ω the physical frequency. Plotting $|A(\omega)/\omega|$ versus $\ln(\omega)$, one again observes the spectrum to be divided into almost identical bands flanked by strong peaks. However, the self-similarity is now asymptotic to the low-frequency side of the spectrum. The peaks in the low-frequency side are generated when $K = 1$ is approached. One can divide all the peaks in the spectrum into "generations." Within each generation, the ratio of any two peaks is an integral power of the golden mean. The classification into generations proceeds through the following scheme: all the peaks in the spectrum can be obtained through the formula $\omega = |m\sigma_G - n|$ where m, n ($m > n$) are successive numbers in Fibonacci sequences with different seeds. For example, generation 1 is obtained by the seed (1,1), generation 2 by the seed (2,2), generation 3 by (1,3), generation 4 using (3,3) and so on.

One, of course, expects the same overall behavior for any irrational ρ with a periodic continued-fraction representation. A renormalization-group calculation of the spectrum has recently been performed.²⁴

In physical terms, an experiment described by a circle map is expected to show correlations over longer and longer time scales as the critical point $K = 1$ is approached. One also expects to encounter the same type of temporal self-similarity if the spectrum of the experimental signal is rescaled accordingly.

The picture of the approach to chaos that we have just described is very reminiscent of the well-known scenario of second-order phase transitions in critical phenomena. In the latter case, the correlation length diverges at the

critical point. This length measures the size of regions in the system over which the order parameter is correlated. In our dynamical system, instead of having a diverging length scale the correlation increases over longer time scales. Smaller frequencies are generated by the system as the transition to chaos is approached.

It is then natural to ask whether the renormalization group applied to dynamical systems could be as successful a technique as it is in the study of critical phenomena. The answer hinges on whether scaling behavior can be observed in the particular problem. The work of Feigenbaum has shown that the answer is positive in the case of period doubling.⁴

Strong evidence of scaling for the circle map was first found by Shenker. Renormalization-group analyses by other authors appeared soon afterward.⁵⁻⁷

In analogy to Feigenbaum's indices α and δ , scaling indices were also defined for the circle map. For a given value of K , denote by $\Omega_i(K)$ the value of Ω such that there is a cycle with winding number ρ_i passing through $\theta = 0$. Shenker defined the index δ as a measure of the convergence of the sequence Ω_i ,

$$\delta(K) = \lim_{i \rightarrow \infty} \left[\frac{\Omega_{(i-1)}(K) - \Omega_i(K)}{\Omega_i(K) - \Omega_{(i+1)}(K)} \right].$$

He found a nontrivial value of $\delta(K)$ for $K = 1$. If d_i represents the distance modulo 1 between $\theta = 0$ and the closest element on the q_i cycle closest to it, the index $\alpha(K)$ was defined by

$$\alpha(K) = \lim_{i \rightarrow \infty} \left[\frac{d_{i-1}}{d_i} \right].$$

Again, a nontrivial value was found when $K = 1$. The values of $\alpha(K)$ and $\delta(K)$ at $K = 1$ are denoted simply by α and δ . These depend upon the irrational winding number ρ chosen to approach the $K = 1$ line. Therefore α and δ are local properties of the critical line as opposed to its fractal dimension, which is a global property.

In contrast to period doubling, where both the critical indices are readily obtained from experimental data, only δ can be measured directly from the quasiperiodicity experiment. To do this, one interprets the Ω_i in the definition of δ as the locked-state widths at the critical line. The justification for this procedure can be found in Jensen, Bak, and Bohr.²¹

To measure α , one has to resort to a more involved analysis of the data.²⁵ This has recently been done using the idea that the attractors in phase space can be described as interwoven fractal sets of singularities.^{26,27} Since this development is quite recent and well documented, we will not dwell on it and refer the reader to the above-cited literature.

III. THE EXPERIMENT

A. Effect of a magnetic field on convection

In this section we present in detail our experimental system. We start by describing the influence of the magnetic field on the convection of an electrically conducting

fluid. This has been studied before, and we present here only a summary of these ideas and results. We then describe in detail the geometry of our cell and finish by giving a description of the overall setup.

In our experiment we used mercury as a convective fluid. The purpose is twofold. First, mercury has a small Prandtl number $P=0.025$. Second, mercury is an electrical conductor. We used the latter property to introduce the external excitation into the system by passing an ac current through the fluid. Since the experiment was embedded in a magnetic field, an ac Lorenz force acted on the fluid. There are two main reasons for using electromagnetic methods to excite the system as opposed to thermal ones. First, the response and relaxation times are much faster in the former case: a couple of minutes versus about one hour for thermal methods. In the thermal-method case, the heat excitation can only be applied through the boundaries of the cell and has to diffuse across the bulk. Since this diffusion time is of the order of the motion time scale, one introduces a phase lag between the internal mode and the excitation. Moreover this phase lag is space dependent. On the other hand, an electromagnetic excitation can act directly on the bulk with negligible phase lag. But most important, with an electromagnetic excitation one acts directly on the velocity field instead of acting on it indirectly through the temperature field. In particular, one can devise a geometry for currents and field so that the excitation will induce vertical vorticity in the flow.

As mentioned in Sec. II A, for low-Prandtl-number fluids like mercury the first instability of the convection pattern when R is increased is the oscillatory instability. The action of a horizontal magnetic field on an electrically conducting convective fluid has already been investigated.^{28,29}

In a theoretical description of the problem, one augments the Navier-Stokes equation with a term $\mathbf{j} \times \mathbf{B}$ where \mathbf{j} is the induced current in the fluid due to the motion of charges in \mathbf{B} . One adds to the Navier-Stokes and Fourier equations an equation describing the evolution of the field,

$$\partial_t \mathbf{B} = \nabla \times (\mathbf{u} \times \mathbf{B}) + \nu_m \nabla^2 \mathbf{B},$$

where the magnetic viscosity ν_m is $1/(\sigma\mu)$, σ being the electrical conductivity and μ the magnetic permeability. This equation is derived from Maxwell's equations after neglecting the displacement current. This effectively adds to our two nondimensional parameters R and P a nondimensional number Q called the Chandrasekhar number.³⁰ Q contains the effect of the field,

$$Q = \frac{\sigma B^2 d^2}{\rho \nu}.$$

Given the length and velocity scales of the flow in our experiment and the electrical conductivity of mercury, the diffusion term in the field equation dominates over the advection term in the right-hand side. Moreover, the magnetic time scale of the problem is $d^2/\nu_m \sim 10^{-3}$ sec for $d=7$ mm whereas the thermal timescale is $d^2/\kappa \sim 10$ sec. The field then relaxes much faster than a thermal disturbance so it does not contribute in a significant way

to the dynamics of the problem.

Another important result concerning convection in a magnetic field is the analogue of the Taylor-Proudman theorem for convection in a rotating layer. The mathematical expression of this result is

$$(\mathbf{B} \cdot \nabla) \mathbf{u} = 0.$$

The physical significance of this result is that any velocity gradient in the direction of the field will be considerably damped.

For a horizontal field, this result implies that the convection rolls will have their axes aligned parallel to the field. Also, instabilities for which the rolls deform transversely to the field will be inhibited. For the oscillatory instability in particular, we can then expect its onset to be pushed up in R and that its frequency will be increased. This has been verified both theoretically and experimentally. The experimental results are in agreement with the following theoretical predictions:

$$R_Q^{(OI)} - R_{Q=0}^{(OI)} \propto Q,$$

$$f_Q^{(OI)} - f_{Q=0}^{(OI)} \propto Q,$$

where $R^{(OI)}$ and $f^{(OI)}$ are, respectively, the Rayleigh number and frequency at the onset of the oscillatory instability.

B. The cell

Our Rayleigh-Bénard cell is depicted in Fig. 2. Its height is $d=0.7$ cm, length $2d$, and width d so that it can support two convective rolls. Its lateral boundaries are made out of Plexiglass while the bottom and top plates are made out of copper. The heat conductivities at 300 K of these materials are given in Table I.

The copper surfaces were covered with a very thin layer of paint in order to avoid chemical contact between the mercury and the copper.

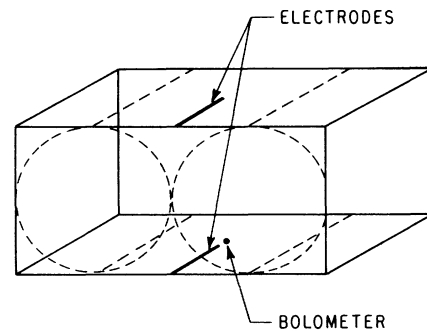


FIG. 2. Schematic diagram of our Rayleigh-Bénard cell. The dimensions of the cell are height $d=7$ mm, width d , and length $2d$. Two convective rolls fit in the cell and are depicted by dashed lines. The electrodes through which an electrical current is passed are shown by bold lines. Notice they cross only up to half the cell's width. An experimental signal is taken out from the experiment through a bolometer located at the center bottom of the cell. The cell is embedded in a magnetic field parallel to the rolls' axes.

TABLE I. Thermal conductivities at 373 K of mercury and the materials used to build the cell's bounding surfaces.

Material	Thermal conductivity (W/cm K)
Mercury	0.085
Copper	4.01
Acrylic (Plexiglass)	2×10^{-3}

Two thin line electrodes were attached to the horizontal surfaces on top of the paint layer. Although the wires crossed the cell completely, their insulation was stripped over half the cell's width, as depicted in the figure.

An ac pulsed current sheet was then passed through the electrodes via the copper plates, the top one of which was grounded. The current consisted of rectangular pulses whose width was set to about $\frac{1}{10}$ the period of the oscillatory instability, i.e., about 0.40 sec. A typical value for the pulse amplitude was 20 mA. The pulses were obtained by reshaping a square wave signal from a Hewlett-Packard HP-3325A function generator with an analog circuit. This circuit allowed us to change the duty cycle smoothly.

The whole setup was embedded in a horizontal magnetic field of 200 G strong parallel to the short side of the cell. The ac Lorenz force acting on the fluid was then horizontal and transverse to the rolls' axes. Notice that with the electrode geometry described above, the action of the Lorenz force is to bend the convection rolls, thereby creating an ac vertical vorticity component in the flow. Had the effective length of the electrodes been equal to the width of the cell, one roll would have been compressed while the other would have been expanded according to the force's phase. This, of course, does not induce any vertical vorticity.

The fact that the excitation induces vertical vorticity in the flow allowed us to couple it dynamically with the oscillatory instability. This assertion was confirmed experimentally by making power spectra of a temperature signal obtained from the cell. In the case of the electrodes having length d , both the oscillatory instability and the excitation peaks were observed in the spectrum but no combination peaks appeared. Thus the oscillators were not dynamically coupled. On the other hand, when the electrodes length was $d/2$ as in Fig. 2, strong combination peaks appeared.

Other types of excitations were also considered and tried but with negative results. Among these, the most notable is one in which instead of acting on the vertical vorticity we acted directly on the velocity field. This was achieved by putting two vertical electrodes in the middle of the long side of the cell, and aligning the horizontal field perpendicular to the rolls. In this case the Lorenz force was vertical and acted along the plane dividing the two rolls. The force accelerated or retarded the rolls velocity depending upon the phase.

In the initial trials of the experiment a sinusoidal excitation was used. While a very strong coupling between

the excitation and the oscillatory instability was observed for the 1/1 tongue, no other tongues were found when sweeping with the external frequency. In addition, as the amplitude of the injected current was increased, the excitation completely dominated the flow before any interesting dynamical behavior was observed.

We then tried an ac current of small duty-cycle pulses. The motivation for this was that since no force acts on the fluid between pulses, time is left for the fluid to relax after each pulse. With a sinusoidal excitation, a force acts on the fluid essentially at all times.

The temperature signal was obtained from a negative temperature resistance (NTR) thermistor located at the center of the bottom plate. Its linear dimensions are 0.03 cm and it was implanted in the copper through a 1-mm hole filled with high-thermal-conductivity stycast. The thermistor was part of a bridge and lock-in detection was used to amplify the signal for further processing.

The temperatures of the top and bottom plates were monitored by platinum bolometers implanted in the copper plates. Heat was applied to the cell by passing a regulated current through a heating coil attached to the bottom plate.

C. The setup

The overall setup is shown in Fig. 3. Both the Plexiglass cell and the lower plate were enclosed by a brass can anchored thermally and mechanically to the upper copper plate. There was no thermal contact between the can and either the Plexiglass cell or the lower copper plate.

Since the temperature of the upper copper plate was kept constant up to 1×10^{-3} °C, the can's temperature was constant as well. The can therefore worked as a constant temperature radiation shield so that a dynamic equilibrium in radiation flux to and from the lower plate could be maintained. A brass thermal resistance with a water jacket on its top was attached to the top copper plate.

Since the whole system was enclosed by a vacuum can, the water jacket provided the only means of taking heat

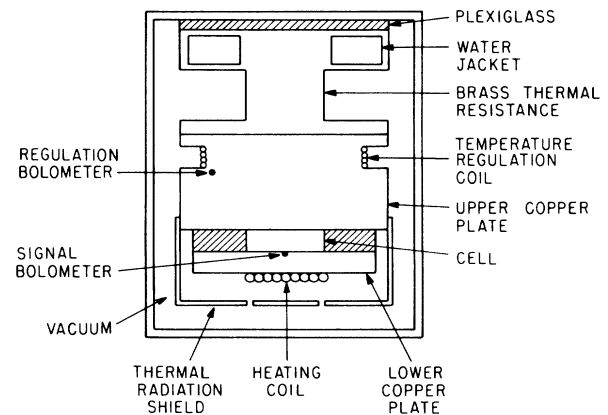


FIG. 3. Our experimental setup. For details see text.

out of the system. A Plexiglass plate was located between the brass resistance and the vacuum can to isolate the system from thermal disturbances in the can. The brass thermal resistance and the upper copper plate acted like a low-pass thermal filter. They filtered out fast variations in the room temperature and in the cooling rate due to temperature and pressure changes in the water line.

In the experiment, only the temperature of the upper plate is regulated. A heating coil is located at the top of the upper plate for this purpose. A platinum bolometer was inserted in the copper plate as near as possible to the coil as part of the regulation loop.

We end this section by noting some important points concerning our temperature regulation. Because of the geometry of our cell and the thermal conductivities of mercury and Plexiglass, practically all the heat supplied through the bottom plate goes through the mercury. In other words, the thermal impedance of the walls is much higher than that of the mercury. Since a constant current is applied to the heating coil of the lower plate and only the temperature of the upper plate is regulated, we are effectively controlling the heat flux through the cell. Using an analogy with an electrical circuit, we have then a "constant current" situation instead of a "constant voltage" (constant ΔT).

As mentioned above, the temperature of the upper plate is constant up to $1 \times 10^{-3} \text{ }^\circ\text{C}$ which means a temperature stability of better than 10^{-5} . A good temperature regulation is essential in this experiment since the stability of the oscillatory instability depends on temperature, in particular its frequency (see Sec. II A). In our case, a change of $1 \times 10^{-3} \text{ }^\circ\text{C}$ induced a change of $10 \text{ } \mu\text{Hz}$ in the frequency of the oscillatory instability.

IV. RESULTS

A. Preliminaries

In our cell, convection starts when the temperature difference between the upper and lower plates is $3.0 \pm 0.1 \text{ }^\circ\text{C}$. This defines our critical Rayleigh number R_c . The critical-temperature difference was determined from Nusselt-number measurements. One then increases the temperature difference until a well-defined oscillatory instability appears in the flow. As explained in Sec. III A, both the onset of the oscillatory instability and its frequency depend upon the applied magnetic field.

If R_{OI} denotes the Rayleigh number at which the oscillatory instability appears, then the change of R_{OI} with the field is given in our system by

$$\frac{1}{R_c} \frac{\Delta(R_{OI} - R_c)}{\Delta B} = 2.8 \times 10^{-3} \text{ G}^{-1}.$$

If $\omega_{OI}^{(0)}$ is the frequency of the oscillatory instability at zero magnetic field, then the relative change in frequency with field is

$$\frac{1}{\omega_{OI}^{(0)}} \frac{\Delta\omega}{\Delta B} = 4 \times 10^{-4} \text{ G}^{-1}.$$

With a field of 200 G, the oscillatory instability appeared at $11.9 \text{ }^\circ\text{C}$ with a frequency of $\omega_0 = 230 \text{ mHz}$. This rela-

tively small value of the field was chosen in order for the signal to be as simple as possible in its harmonic content. For higher values of the field ($B \approx 800 \text{ G}$) the signal acquires a strong $2\omega_0$ component.

Since the oscillatory instability appears through a Hopf bifurcation, it starts from zero amplitude. Eventually its amplitude saturates when R is increased enough above R_{OI} .

A second oscillatory mode appears in the flow if R is further increased. We therefore set R below the onset of this secondary mode but in the range of saturation of the oscillatory instability. This still leaves a large range of variation for R . It turns out that a more stringent lower bound has to be imposed on R . We have found that if the oscillatory instability does not have a high enough amplitude, the excitation starts to dominate completely the behavior of the flow before the transition to chaos takes place. The way in which this happens is detailed in Sec. IV B. An oscillatory mode with an amplitude of 70 dB above noise level or higher suffices to reach a chaotic regime. This amplitude can be achieved by adjusting the Rayleigh number and the magnetic field.

Once the amplitude of the oscillatory instability has the required value, the experiment can proceed. One chooses a particular frequency ratio ω_0/ω_e and tunes the external frequency ω_e to get this ratio. This tuning is nontrivial since the introduction or change in the excitation alters the frequency of the oscillatory instability. One has therefore to tune ω_e iteratively two or three times until one achieves the desired accuracy in the frequency ratio. In our case we can achieve a precision of 10^{-5} . We explain now the different procedures we have used to perform the tuning.

For low amplitudes of the injected current, we have used a fast Fourier transform of the signal and monitored the frequency of the internal and external oscillators.

For current amplitudes near the critical line, the easiest and fastest method is to follow the sequence of locked states corresponding to the rational approximants of the irrational number chosen. This method works well on the critical line since all the locked states cover it except for a set of measure zero. For example, in our experiment we can clearly resolve the locked state $\frac{89}{144}$ which is a rational approximant to σ_G . The difference between this rational number and σ_G is 2×10^{-5} . It should be nevertheless clear that in a physical experiment, irrational winding numbers cannot be obtained. The best one can do is to approximate them with a rational ratio.

The third procedure to calibrate the frequency ratio is due to Thomae.³¹ The idea is to strobe the signal with the excitation's frequency and plot the points in a computer screen versus points generated by a uniform rotation $s_{\tau+1} = s_\tau + \rho$. One then varies ρ until a well-defined curve is traced. Even tiny differences between ρ and the experimental frequency ratio lead to a considerably blurred curve. The procedure is nothing more than a Lissajous figure. It allows a determination of the frequency ratio with an accuracy of 2×10^{-6} . This method has been used to monitor the drifts in the experiment due to limitations in temperature stability.

As mentioned before, $1 \times 10^{-3} \text{ }^\circ\text{C}$ change in temperature

changes ω_0 by $10 \mu\text{Hz}$. Therefore changes in the frequency ratio are observable.

B. Local results

Starting with a small amplitude in the injected current, we tuned the frequency ratio to $\sigma_G \pm 10^{-4}$. Without the excitation, the oscillatory instability had a frequency of 230 mHz. We then progressively increased the amplitude of the excitation, keeping at each step the frequency ratio constant within 10^{-4} . We present in Fig. 4 three spectra for various values of the current amplitude. These spectra have been presented previously.¹¹

In Fig. 4(a), we show a typical spectrum for small current amplitude ($I = 16.9 \text{ mA}$). One sees the oscillatory instability and excitation peaks plus other peaks corresponding to frequencies of the form $\omega = m\omega_0 + n\omega_e$. Here m, n are integers which in this case are small. As the current amplitude is increased, the height of all the spectral peaks increases and new peaks corresponding to combinations with larger m and n appear.

This trend continues with increasing excitation. But there exists a value of the excitation above which the oscillatory instability and the combination peaks start shrinking. At the same time the excitation peak continues to grow. The excitation at this point is strong enough to disrupt the oscillatory instability mode and it starts to

dominate the dynamical behavior. Further increases of the injected current enhance this phenomenon. Eventually, the excitation completely dominates the flow, and it is the only peak in the spectrum.

The value of the current amplitude at which this phenomenon appears depends on the amplitude of the oscillatory instability at which one starts the experiment. For this phenomenon to occur after the transition to chaos has taken place, we need an amplitude larger than 70 dB for the oscillatory instability.

In Fig. 4(b) we show a spectrum for $I = 17.4 \text{ mA}$. The peak population has greatly increased. Finally in Fig. 4(c) we show a spectrum for $I = 21.5 \text{ mA}$. High-order combination frequencies are weaker and broadband noise has started to rise with an average increase of 20 dB. The spectrum in Fig. 4(b) is a good approximation to the critical line. In fact, one can find the critical line with great precision by rescaling the spectrum as explained in Sec. II B. As the critical line is approached, more and more self-similar bands appear in the spectrum in the low-frequency region. At the same time, peaks belonging to the same generation tend to have the same rescaled amplitude. We show such a rescaled spectrum corresponding to Fig. 4(b) in Fig. 5. We plot $\log_{10}[P(\omega)/\omega^2]$ versus $\log_{10}\omega$. Not all the peaks appearing in Fig. 4(b) appear in the rescaled spectrum for the sake of clarity. Apart from the oscillatory instability and excitation peaks, one can observe six peaks belonging to generation one, all of which have nearly the same amplitude. Generations of order higher than 1 do not appear in the low-frequency side of the spectrum. Moreover, the constant-amplitude criterion for these is less well obeyed.

We have lately been able to get a better approximation to the critical line. We present our best spectrum in Fig. 6. Notice that the excitation peak does not appear in the

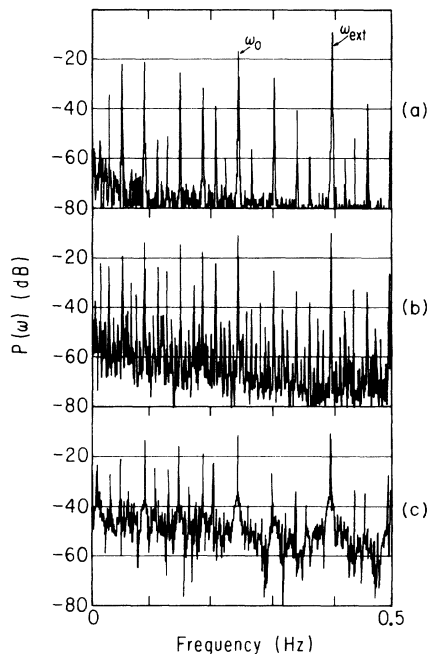


FIG. 4. Spectra $\log P(\omega)$ vs ω for quasiperiodic states with frequency ratio $\omega_0/\omega_e = \sigma_G \pm 2 \times 10^{-4}$, where ω_0 is the frequency of the oscillatory instability and ω_e the excitation's frequency. The spectra were taken when the Rayleigh number was fixed to be $R = 4R_c$. Each spectrum corresponds to a different amplitude of the injected pulsed current: (a) $I = 16.9 \text{ mA}$ below the critical line, (b) $I = 17.4 \text{ mA}$ good approximation to the critical line, and (c) $I = 21.5 \text{ mA}$ above the critical line.

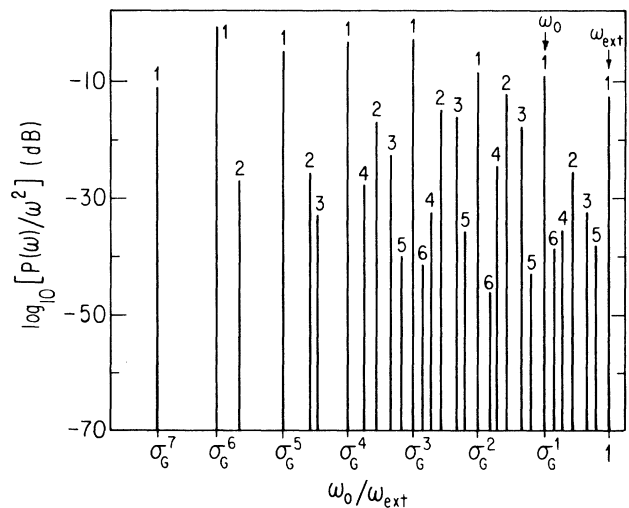


FIG. 5. Rescaled version of the spectrum in Fig. 4(b). We plot $\log P(\omega)/\omega^2$ vs $\log(\omega)$. Not all the peaks in Fig. 4(b) appear in this figure for the sake of clarity. Each peak is labeled by an integer specifying the generation to which it belongs.

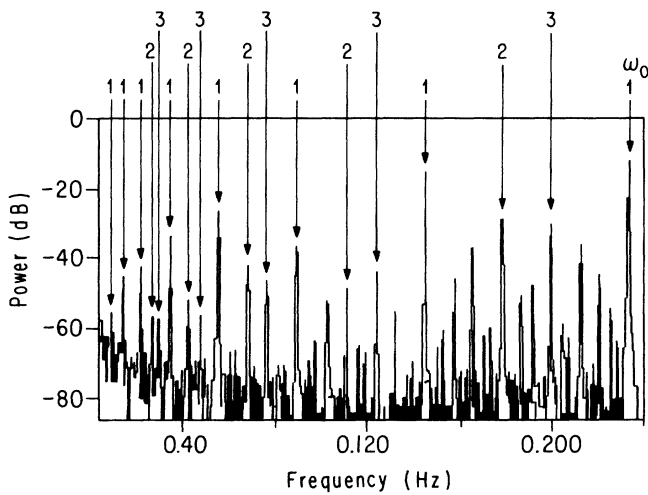


FIG. 6. Power spectrum for a quasiperiodic state with frequency ratio $\sigma_G \pm 1 \times 10^{-4}$. This spectrum represents the nearest approximation to the critical line obtained from our experiment. Notice that the excitation's peak does not appear given the bandwidth of the spectrum. Peaks can be classified into generations, and we indicate by means of dotted arrows the peaks belonging to the first three generations.

bandwidth chosen. Figure 7 shows an expanded view of the low-frequency portion of Fig. 6. Not counting the oscillatory instability peak, we now have nine peaks belonging to the first generation falling near Fibonacci frequencies. One can also observe the self-similar structure of the spectrum at lower frequencies than for the case of Fig. 4(b).

We have approached the critical line through a different irrational route, namely, the silver mean σ_S . In Fig. 8 we show both the normal power spectrum and its rescaled version in a good approximation to the critical line.

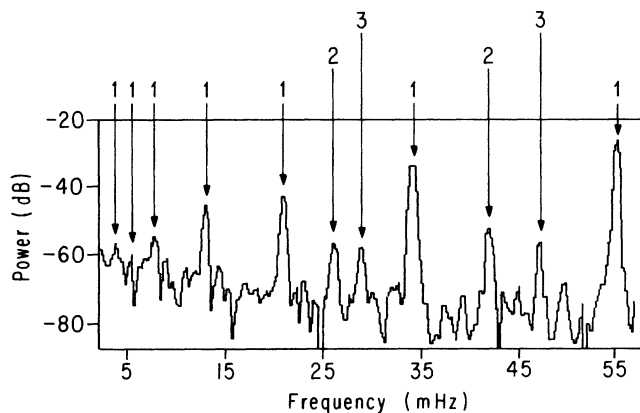


FIG. 7. Blow up of the low-frequency side of the power spectrum shown in Fig. 6. One can observe here additional peaks belonging to generations 1, 2, and 3 which do not appear in Fig. 6.

Figures 6 and 8 were not obtained in the same experimental run. If one performs these measurements on the same run, one can map out the position of the critical line. We have done this for both σ_G and σ_S . Our results clearly show that the critical line is not a line of constant current amplitude. We present these results in Sec. IV D in our discussion of the parameter-space current versus external frequency (I, ω_e) .

We have performed Poincaré cross sections of the experimental data to see how the transition manifests itself in phase space. To do this, we strobe the experimental signal at the frequency of the excitation. In the right-hand part of Fig. 9 we show three-dimensional phase portraits for the golden-mean route. The left side of the figure contains the Lissajous figures used to determine the winding number of the particular state. The limit cycles have been drawn as lines and not as a set of points since an averaging and interpolation procedure has been applied to the data. This figure has been adapted from Ref. 24. Three cases are presented in this figure: small excitation $I = 2.26$ mA, intermediate amplitude $I = 7.82$ mA, and near-critical amplitude $I = 11.81$ mA.

By rotating these figures on the computer screen, we have checked that all these phase-space trajectories do not self-intersect when the embedding space of the experimental points is three dimensional. We have verified this for the σ_S case as well. All the limit cycles in Fig. 9 are closed, nonintersecting curves and are topologically equivalent to a circle. Of course, we expect this since below criticality the dynamics of our problem is topologi-

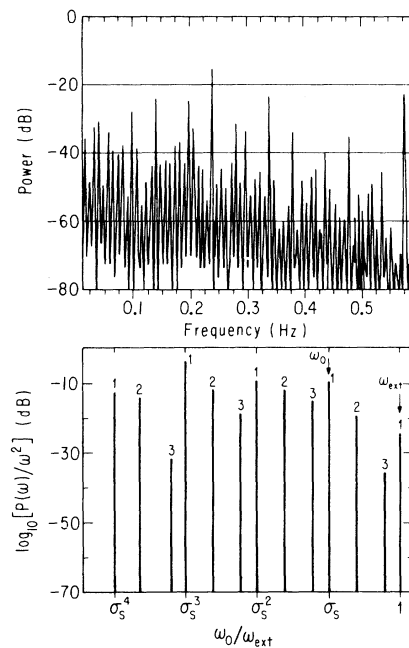


FIG. 8. Power spectrum and its scaled version (up to generation 3) for a quasiperiodic state with frequency ratio $\sigma_S \pm 2 \times 10^{-4}$. The amplitude of the injected current is $I = 25.2$ mA. The state was obtained for $R = 3.98R_c$.

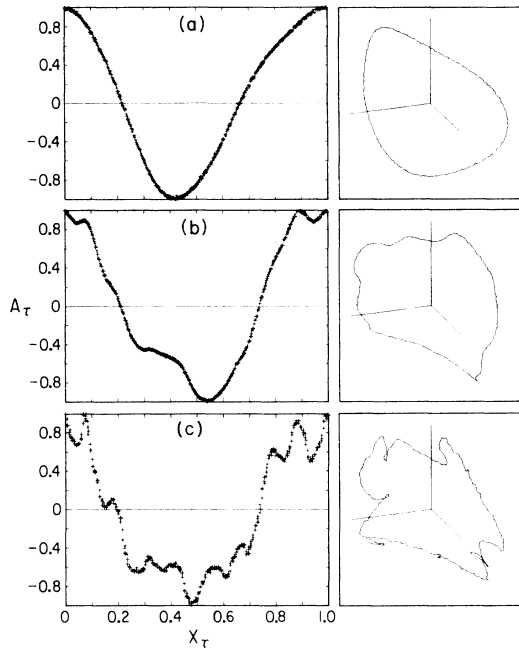


FIG. 9. Strobbed signal A_τ vs uniform rotation generated points x_τ and corresponding limit cycles in three-dimensional phase space $(A_{\tau+2}, A_{\tau+1}, A_\tau)$. The states have a frequency ratio of $\sigma_G \pm 2 \times 10^{-4}$ and correspond to the following injected current amplitudes: (a) 2.26 mA (low amplitude), (b) 7.82 mA (intermediate amplitude), and (c) 11.81 mA (good approximation to the critical line).

cally conjugate to that of a uniform rotation. For small amplitudes, the trajectory is very simple. As the current amplitude increases, the trajectory wrinkles more and more. However, given our accuracy, we are not able to see whether a fractal structure develops.

For comparison we plot in Fig. 10 two-dimensional phase portraits $x_{\tau+1}, x_\tau$ for different current amplitudes in the case of the silver mean. No averaging or interpolation procedure has been applied in this case. The figure shows phase portraits below, near, and above criticality. The first feature to catch one's attention is that the limit cycles for σ_S are much more contorted than those for σ_G . This may be due to the following reasons. The convergence of the rational approximants to the silver mean is much faster than that of σ_G . In the parameter space (I, ω_e) , the tongues corresponding to these rational approximants will be more closely clustered around the σ_S line than for σ_G . By the same token, we expect that in phase space the basins of attraction of these different locked states will be more closely interwoven. Since the irrational limit cycle avoids these basins of attraction, it must necessarily be more contorted.

Another important feature observed in this figure is that above criticality, the trajectory seems space filling. We do not expect a simple, closed nonintersecting trajectory since the equivalence with a uniform rotation does not hold in this case. Nevertheless, one should keep in mind other alternative explanations, such as a possible

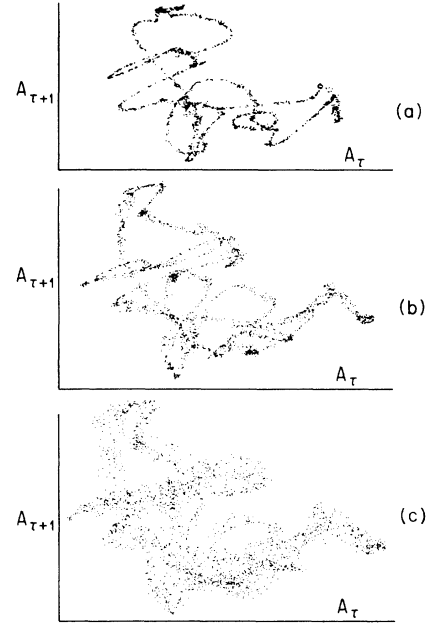


FIG. 10. Two-dimensional phase spaces $(A_{\tau+1}, A_\tau)$ for states with frequency ratio of $\sigma_S \pm 2 \times 10^{-4}$ and different amplitudes of the injected pulse current: (a) below criticality, (b) near criticality, and (c) above criticality.

breakdown of the description of the experiment by a one-dimensional map. If this is indeed the case, one should find a different behavior in the rich bifurcation structure within locked states above criticality. Results concerning this problem have already been published elsewhere.³²

C. Scaling behavior

In Sec. IV B we presented spectra at the critical line for both the golden and silver mean. The qualitative features

TABLE II. Frequency limits of locked states near σ_G and σ_S at the nearest approximation to the critical line. The frequencies were obtained at $I = 17.4$ mA and $R = 4.09R_c$ for σ_G , and at $I = 19.4$ mA and $R = 3.94R_c$ for σ_S .

Locked state	ω_{low} (mHz) $\sigma_G = \langle 1, 1, 1, 1, \dots \rangle$	ω_{high} (mHz)
$\frac{13}{21}$	392.350	392.663
$\frac{21}{34}$	393.230	393.345
$\frac{34}{55}$	393.050	393.095
$\frac{55}{89}$	393.133	393.150
	$\sigma_S = \langle 2, 2, 2, 2, \dots \rangle$	
$\frac{12}{29}$	574.175	574.575
$\frac{17}{41}$	573.450	573.650
$\frac{29}{70}$	573.865	573.925

TABLE III. Experimental values of the scaling index δ for the irrational trajectories σ_G and σ_S at the corresponding critical current amplitudes.

	$\sigma_G = \langle 1, 1, 1, 1, \dots \rangle$	$\sigma_S = \langle 2, 2, 2, 2, \dots \rangle$
δ	2.8 ($\pm 10\%$)	7.0 ($\pm 10\%$)

of these spectra are the same. It is reasonable to expect the same conclusion for other irrational routes as well, as long as these are characterized by periodic continued-fraction representations.

However, the quantitative characteristics of both spectra are different. The same is true for the scaling properties of these and other irrational routes. In Sec. IIB the scaling indices α and δ were defined. The experimental measurement of δ is straightforward. One needs to measure the widths of tongues corresponding to three consecutive truncations of the continued-fraction representation of a particular irrational. We measured δ around both σ_G and σ_S . In Table II we show the low- and high-frequency limits of the locked states used in the computation of δ . In Table III we present our results and the theoretical predictions from the circle map for both σ_G and σ_S . Within the experimental uncertainty, the agreement is very good. As we mentioned before, the measurement of α is more involved and we refer the interested reader to the paper by Jensen *et al.*²⁵

D. Global results

By varying the amplitude and frequency of the injected current, we mapped out a number of Arnol'd tongues. We show some of these tongues in Fig. 11, where the amplitude of the current is plotted as a function of 1 over its frequency. The normalization factor $\omega_{01}^{(0)}$ corresponds to the frequency of the oscillatory instability at zero excitation.

Within a tongue, the signal is periodic but its line shape changes as the tongue is scanned at constant current amplitude. This happens because the relative phase between the external and internal oscillators changes as the tongue is crossed.

Looking at constant current amplitude lines in Fig. 11, one observes the rapid decrease in the width of the tongues as the denominator increases. It is for this reason that tongues with denominator higher than 5 have not been shown.

Nevertheless, we were able to observe tongues with denominator higher than 200 in a stable way. The slight inclination of the tongues towards lower values of $1/\omega_e$ is due to the decrease in the frequency of the oscillatory instability as the amplitude of the excitation is increased.

One also observes that the width of a given tongue increases with the current amplitude. Since this is true for all tongues, they eventually overlap at some critical current amplitude. This critical current amplitude is dependent on the winding number. By using the procedures outlined in Sec. IV B, we have found the position of the critical line for σ_G and for σ_S . This is indicated in Fig. 11 by the origins of the two insets.

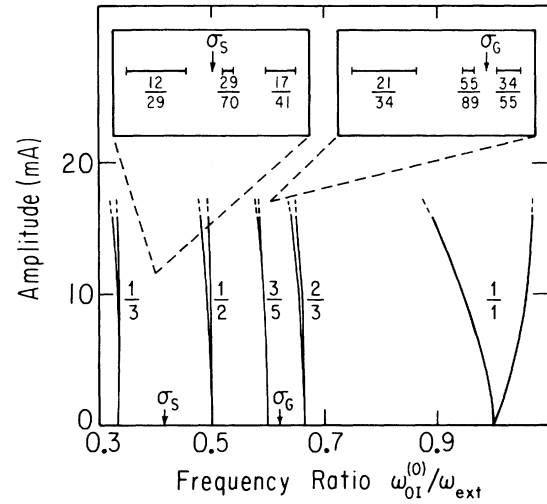


FIG. 11. Parameter space $(I, \omega_{01}^{(0)}/\omega_{\text{ext}})$ where I is the amplitude of the current injected into the system, ω_{ext} its frequency, and $\omega_{01}^{(0)}$ the frequency of the oscillatory instability at zero current as normalization. The diagram shows only Arnol'd tongues of appreciable width with their corresponding winding numbers. Insets: locked states near σ_G and σ_S on the critical line. The origin of each inset shows the position of the critical line at the particular frequency ratio. For the exact frequency limits of each of these states see Table II.

The tongues interpolate between the zero amplitude line where the locked states have zero width, and the critical line where they fill it, up to a set of zero measure. This set of zero measure and the critical line has a fractal structure and hence can be characterized by its fractal dimension D^* . A good approximation D to D^* can be obtained by the following algorithm.³³ Denote by S the length of the interval between two locked bands on the critical line. This interval contains inside it the locked band corresponding to the Farey composition of the two flanking locked states. Denote by S_1 and S_2 the length of the intervals between the daughter state and each of its parents. Then D is given by

$$\left(\frac{S_1}{S}\right)^D + \left(\frac{S_2}{S}\right)^D = 1.$$

A more accurate approximation to D^* would involve taking more subintervals S_i by generating more daughters by the Farey scheme. It turns out that for the circle map the difference between D^* and D is $\sim 3\%$.

Taking our data from Table II we computed D near σ_G and σ_S . Our results are displayed in Table IV. Within the experimental error, the results are the same confirm-

TABLE IV. Experimental values for the fractal dimension of the critical line obtained near σ_G and σ_S .

	$\sigma_G = \langle 1, 1, 1, 1, \dots \rangle$	$\sigma_S = \langle 2, 2, 2, 2, \dots \rangle$
D	0.86 ($\pm 3\%$)	0.85 ($\pm 3\%$)

ing that D^* is a global property of the critical line. Second, they compare well with the theoretical prediction $D = 0.868 \dots$

V. CONCLUSIONS

From a theoretical standpoint, we have drawn three main conclusions from our study.

As in the case of period doubling, we have shown that the theory of dynamical systems provides a good framework for understanding the time dynamics of small-aspect-ratio fluid systems.

Second, our assumption of universality proved to be a good one. Below and at the transition to chaos, the circle map, simple though it may be, accounts qualitatively and quantitatively with the dynamical behavior of the huge number of degrees of freedom of the moving fluid, regardless of their interaction. The same fact has been verified in quasiperiodicity experiments in strikingly different systems such as electron plasmas in semiconductors.^{34,35}

Third, our results show that the quasiperiodic transition to chaos is indeed a phase transition of the second kind. In critical phenomena, the transition is associated with the divergence of the correlation length as the critical point is approached. Our system shows correlation over longer time scales as the critical line is approached. Moreover, critical indices can be defined and measured in our case.

From the experimental and hydrodynamical point of view, we would like to emphasize the following points. There is a definite requirement for the amplitudes of the oscillators in an experiment, in order for the transition to chaos via quasiperiodicity to be observed. These amplitudes must be high enough in order to feed the multitude of composite modes represented in the Fourier spectrum at the transition. As our results in Sec. IV show, the critical point can be regarded as a multicritical point in a generalized parameter space with the amplitudes and frequencies of both oscillators as the axes. There is a surface transversal to the amplitude axes dividing this space in two regions. In one region, the oscillators have small amplitudes whereas in the other, the system is characterized by large amplitudes. The critical point is in the large-amplitude region. If the system is in the small-amplitude region, one can get near the critical point but eventually one falls into one of its unstable manifolds and the transi-

tion is not observed.

If on the other hand one is in the large-amplitude region, one can fall on the stable manifold of the critical point and the transition is observed. Hence, the surface dividing the small- and large-amplitude regions is the locus of the minimal amplitudes the oscillators must have in order for the transition to chaos to be observed. These minimal amplitudes are winding-number dependent.

We have experimentally demonstrated the connection between the oscillatory instability and vertical vorticity. Of all the different ways we tried to excite our system, the one that induced vertical vorticity caused dynamical coupling with the oscillatory instability.

Moreover, we have shown how the velocity and temperature fields are intimately connected. Our excitation acted on the velocity field which in turn acted on the temperature field through the nonlinear term in the Fourier heat equation.

Last, we would like to draw attention to the remarkable accuracy at which a well-controlled hydrodynamical system can be driven.

Some aspects of the experiment should be pursued in the future. A detailed study of the region above the critical line should be performed. Although the bifurcation structure of a tongue has already been studied,³² a study of other tongues as well as the chaotic regions is lacking.

ACKNOWLEDGMENTS

My warmest thanks go to Professor Albert Libchaber, who suggested the present experiment, and for his patience, advice, and support during all the stages of the project. I wish to thank particularly Francois Heslot for his constant help and for teaching me the nuts and bolts of experimental physics. Very stimulating discussions with L. P. Kadanoff, I. Procaccia, M. Jensen, S. Thomaé, B. Shraiman, and J. Glazier are acknowledged. This work was supported by National Science Foundation (NSF) Grant No. DMR-83-16204 and the Materials Research Laboratory at the University of Chicago under NSF Grant No. DMR-82-16892. This work is presented as a thesis to the Department of Physics, The University of Chicago, in partial fulfillment of the requirements for the Ph.D. degree.

*Address from October 1986: Department of Physics, University of Pittsburgh, Pittsburgh, PA 15260.

¹V. I. Arnol'd, *Transl. Am. Soc.*, 2nd Ser. **46**, 213 (1965).

²M. R. Herman, *Geometry and Topology*, Vol. 597 of *Lecture Notes In Mathematics* (Springer, Berlin, 1977).

³A. Denjoy, *CR Acad. Sci.* **195**, 478 (1932).

⁴M. J. Feigenbaum, *J. Stat. Phys.* **21**, 669 (1979).

⁵D. Rand, S. Ostlund, J. Sethna, and E. D. Siggia, *Physica* **8D**, 303 (1983).

⁶M. J. Feigenbaum, L. P. Kadanoff, and S. J. Shenker, *Physica* **5D**, 370 (1982).

⁷B. Shraiman, *Phys. Rev. A* **29**, 3464 (1984).

⁸M. H. Jensen, P. Bak, and T. Bohr, *Phys. Rev. Lett.* **50**, 1637

(1983).

⁹S. J. Shenker, *Physica* **5D**, 405 (1982).

¹⁰A. P. Fein, M. S. Heutmacker, and J. P. Gollub, *Phys. Scr.* **T9**, 79 (1985).

¹¹J. Stavans, F. Heslot, and A. Libchaber, *Phys. Rev. Lett.* **55**, 596 (1985).

¹²F. H. Busse, *Rep. Prog. Phys.* **41**, 1929 (1978). This reference contains a comprehensive overview of secondary instabilities.

¹³G. Ahlers and R. P. Behringer, *Phys. Rev. Lett.* **40**, 712 (1978).

¹⁴M. Heutmacker, P. N. Fraenkel, and J. P. Gollub, *Phys. Rev. Lett.* **54**, 1369 (1985).

¹⁵V. Croquette, thesis, Université Pierre et Marie Curie, Paris,

- 1986 (unpublished).
- ¹⁶F. H. Busse, *J. Fluid Mech.* **52**, 97 (1972).
- ¹⁷E. D. Siggia and A. Zippelius, *Phys. Rev. Lett.* **47**, 835 (1981).
- ¹⁸A. C. Newell and J. A. Whitehead, *J. Fluid Mech.* **38**, 279 (1969).
- ¹⁹L. A. Segel, *J. Fluid Mech.* **38**, 203 (1969).
- ²⁰A. Libchaber and J. Maurer, *J. Phys. Lett. (Paris)* **40**, L419 (1979).
- ²¹M. H. Jensen, P. Bak, and T. Bohr, *Phys. Rev. A* **30**, 1960 (1984).
- ²²See, for example, J. Guckenheimer and P. Holmes, *Nonlinear Oscillations, Dynamical Systems and Bifurcations of Vector Fields* (Springer-Verlag, Berlin, 1983).
- ²³P. Cvitanović, M. H. Jensen, L. P. Kadanoff, and I. Procaccia, *Phys. Rev. Lett.* **55**, 343 (1985).
- ²⁴M. J. Feigenbaum, *Nonlinear Phenomena in Physics*, edited by F. Claro (Springer-Verlag, Berlin, 1985).
- ²⁵M. H. Jensen, L. P. Kadanoff, A. Libchaber, I. Procaccia, and J. Stavans, *Phys. Rev. Lett.* **55**, 2798 (1985).
- ²⁶T. C. Halsey, M. H. Jensen, L. P. Kadanoff, I. Procaccia, and B. I. Shraiman, *Phys. Rev. A* **33**, 1141 (1986).
- ²⁷U. Frisch and G. Parisi, in *Turbulence and Predictability in Geophysical Fluid Dynamics and Climate Dynamics*, Proceedings of the International School of Physics "Enrico Fermi," Course LXXXVIII, Varenna, 1984, edited by M. Ghil (North-Holland, New York, 1985).
- ²⁸S. Fauve, C. Laroche, and A. Libchaber, *J. Phys. Lett. (Paris)* **45**, L101 (1984).
- ²⁹F. H. Busse and R. M. Clever, *J. Mech. Theor. Appl.* **2**, 495 (1983).
- ³⁰S. Chandrasekhar, *Hydrodynamic and Hydromagnetic Stability* (Oxford University Press, Oxford, 1961).
- ³¹J. Stavans, S. Thomae, and A. Libchaber, *Dimensions and Entropies in Chaotic Systems*, edited by Mayer-Kress (Springer-Verlag, Berlin, 1986).
- ³²J. A. Glazier, M. H. Jensen, A. Libchaber, and J. Stavans, *Phys. Rev. A* **34**, 1621 (1986).
- ³³See, for example, H. G. E. Hentschel and I. Procaccia, *Physica* **8D**, 435 (1983).
- ³⁴G. A. Held and C. Jeffries, *Phys. Rev. Lett.* **56**, 1183 (1986).
- ³⁵E. G. Gwinn and R. M. Westervelt, *Phys. Rev. Lett.* **57**, 1060 (1986).